Manuscript prepared for Atmos. Chem. Phys. Discuss.
with version 2.2 of the LaTeX class copernicus_discussions.cls.
Date: 29 November 2016

Global distribution of CO_2 in the Upper-Troposphere and Stratosphere

M. Diallo[1,2,7], B. Legras[1], E. Ray[3,4], A. Engel[5], and J. A. Añel[2,6]

[1]Laboratoire de Météorologie Dynamique, UMR8539, IPSL, CNRS/ENS/UPMC/Ecole Polytechnique, Paris, France
[2]EPhysLab, Facultade de ciencias, Universidade de Vigo, Ourense, Spain
[3]Chemical Sciences Division, Earth Systems Research Laboratory, NOAA, Boulder, Colorado, USA
[4]Cooperative Institute for Research in Environmental Sciences,University of Colorado, Boulder, Colorado, USA
[5]Institute for Atmospheric and Environmental Sciences, Goethe University Frankfurt, Frankfurt am Main, Germany
[6]Smith School of Enterprise and the Environment, University of Oxford, Oxford, UK
[7]Institute for Energy and Climate Research - Stratosphere (IEK-7), Forschungszentrum Jülich, Jülich, Germany

Correspondence to: M. Diallo (m.diallo@fz-juelich.de)

Abstract

In this study, we aim to construct a new database of the monthly zonal mean distribution of carbon dioxide (CO_2) at a global scale extending from the upper troposphere to stratosphere. This product is intended for model and satellite validation in the upper troposphere and stratosphere, as a prior for inversion modelling and to analyse features of the stratospheric-tropospheric exchange as well as the stratospheric circulation and its variability. The study is based on the ability of the Lagrangian trajectory model TRACZILLA, driven by ERA-Interim reanalysis to reconstruct the distribution of CO_2 in the upper troposphere and stratosphere. Using 10-year backward trajectories and tropospheric observations of CO_2, we reconstruct upper tropospheric and stratospheric CO_2 over the 2000–2010 period. The reconstruction compares remarkably well with extra-tropical in situ CO_2 observations. The zonal mean distribution shows relatively large CO_2 in the tropical stratosphere due to the seasonal variation of the tropical upwelling of Brewer-Dobson circulation. During winter and spring, the tropical pipe is relatively narrow while it is less confined during summer and autumn. High CO_2 values are more readily transported out of the tropics into the mid and high latitude of the northern lowermost stratosphere around 15 km. Relatively high CO_2 above 20 km altitude is produced by the tropical upwelling. CO_2 mixing ratio is relatively low in the polar and tropical regions above 25 km. On average the CO_2 mixing ratio decreases with altitude by 6–8 ppmv from the upper troposphere to the middle stratosphere (e.g. up to 35 km) and is nearly constant with altitude above 35 km.

1 Introduction

The global stratospheric meridional circulation, also called Brewer-Dobson circulation (BDC), has been recognized as a major component of the climate system, which affects radiative forcing (Lacis et al., 1990; Forster and Shine, 1997; Forster et al., 2007) and atmospheric circulation (Andrews et al., 1987; Holton et al., 1995; Salby and Callaghan, 2005, 2006). The increase of greenhouse gases, in particular carbon dioxide (CO_2) concentration, affects the atmospheric temperature and wave propagation, which increases the tropical upwelling mass flux (Butchart

et al., 2010; Garny et al., 2011; Abalos et al., 2015) and therefore changes the BDC. Within the context of changing climate, the stratospheric circulation variability can be diagnosed using the CO_2 trace gas.

CO_2 is a good and useful tracer of the atmospheric dynamics and transport because of its long lifetime in the troposphere and stratosphere where it has essentially no sources or sinks as it is basically chemically inert in the free troposphere. The only stratospheric source of CO_2 is a small contribution from methane oxidation that can reach up to 1 ppmv (i.e. parts per million per volume) (Boucher et al., 2009). CO_2 is regularly exchanged between four reservoirs: the biosphere (photosynthesis and respiration), the lithosphere (soil and fossil pool), the hydrosphere (surface and deep ocean), and the atmosphere with a much longer residence time in the ocean and soil than in the atmosphere. These exchanges are described as the carbon cycle. Clearly, the anthropogenic emissions, deforestation and biomass and fossil fuel burning have systematically increased the mean CO_2 and modified its seasonal cycle during these last two decades (Tans and Keeling, 2015). With the influences of steady growth and seasonal variation, CO_2 concentrations in the atmosphere contain both monotonically increasing and periodic signals that represent that represents stringent tests of stratospheric transport and Stratosphere-Troposphere Exchange (STE) in models (Waugh and Hall, 2002; Bönisch et al., 2008, 2009).

Despite its potential to increase global change by cooling the stratosphere and warming the troposphere via the greenhouse effect, our knowledge of stratospheric CO_2 and its variability was sparse until recently. In recent years, in situ aircraft and balloon campaigns were held to measure a number of chemical tracers including CO_2. The in situ campaigns included SPURT aircraft measurements in the upper troposphere and lower stratosphere (UTLS) (Engel et al., 2006; Gurk et al., 2008), CONTRAIL (Sawa et al., 2008) and CARIBIC (Schuck et al., 2009; Sprung and Zahn, 2010). Although sporadic in time and space coverage, these in situ measurements have been used to analyse the BDC changes (Andrews et al., 2001a; Engel et al., 2009; Ray et al., 2014), to validate Chemistry-Transport Models (CTMs) (Strahan et al., 2007; Waugh, 2009) and to diagnose STE (Strahan et al., 1998; Bönisch et al., 2009, 2011).

The airborne SPURT campaigns were also used to diagnose the eddy diffusivity in the lowermost stratosphere (LMS) using a 2D-advection-diffusion model (Hegglin et al., 2005) and also

to quantify different transport pathways which contribute to the composition of the LMS over Europe (Hoor et al., 2005, 2010). A main result of the SPURT campaigns has been to document the tropopause chemical transition layer in the extra-tropics.

The stratospheric overworld circulation changes that affect the extra-tropical UTLS were recently assessed by Engel et al. (2009) from balloon-based measurements of SF_6 and CO_2. The stratospheric mean age of air, that is defined as the time residence of air parcels in the stratosphere (Li and Waugh, 1999; Waugh and Hall, 2002; Butchart et al., 2010), was calculated by Ray et al. (2014) from the in situ balloon measurements of trace gases with an idealized model to identify the natural variability in the BDC and its significant linear trends. This study exhibited the importance of reconstructed in situ measurements to validate the stratospheric representation in global CTMs and Chemistry Climate Models (CCMs).

In addition to the very localized in situ observations which have high spatial resolution, a large spatial and temporal coverage of CO_2 is obtained from space instruments such as the vertical nadir sounders TOVS (Chedin et al., 2002, 2003b), AIRS (Chedin et al., 2003a), SCIAMACHY (Bowman et al., 2000), IASI (Chedin et al., 2003a), GOSAT (Hammerling et al., 2012; Liu et al., 2014) and recently OCO-2 (Frankenberg et al., 2015). These spaceborne instruments essentially measure total column CO_2, weighted more by the lower and mid troposphere, hence they bring limited information on the upper troposphere and the stratosphere. Foucher et al. (2009, 2011) have obtained five years of monthly mean CO_2 vertical profiles by analysing the ACE-FTS data (Bernath et al., 2005). This passive space-borne instrument uses the sunset and sunrise to measure the atmospheric chemistry species in limb-view. The main isotopologue $^{12}C^{16}O_2$ was used to retrieve CO_2 in the 10–25 km altitude range and $^{18}OC^{16}O$ in the 5–15 km range when the main isotopologue lines saturate (more detail about the inversion approach is found in Foucher et al. (2009)). The ACE-retrieved CO_2 has shown qualitatively good agreement with in situ observations for 2004–2008 time period and at the 50°N–60°N latitude bins. However, the retrieval sensitivity is limited and averages need to be performed on a large number of profiles.

Because of these limitations in the observations, the CTMs and Lagrangian transport models are a complementary and useful framework to widely diagnose the BDC and to represent the

global transport and distribution of long-lived species, such as CO_2, within the upper troposphere and stratosphere.

Previous studies using the two-dimensional CTM Caltech/JPL (Shia et al., 2006) and the three-dimensional CTM TM5 (Transport Model 5) (Bönisch et al., 2008) were unable to accurately represent the BDC. Bönisch et al. (2008) investigated the UTLS exchanges in a three-dimensional transport model using the observed CO_2 and SF_6 distributions and concluded that major problems occur in winter, where a too strong BDC leads to some overestimates of the CO_2, and in boreal summer, where the vertical transport is too slow in the upper troposphere. During autumn, the models showed an unrealistic persistent reverse gradient in the lower stratosphere and during spring, the transport processes through the tropical tropopause were overestimated, inducing too high CO_2 values in the lower stratosphere. Furthermore, many three-dimensional models are too diffusive and/or have too strong mixing when crossing the tropopause that lead to an underestimation of the amplitude of the seasonal cycle in the column of CO_2 (Olsen and Randerson, 2004). (Shia et al., 2006) suggested that the lack of a reliable representation of stratospheric influence on CO_2, e.g. intrusion and recirculation, could explain part of the discrepancy between a CTM and observations. The persistence of the inverted CO_2 gradient noted in these models can result in an underestimation of the exchange of air masses from the stratosphere to the troposphere in mid-latitudes during fall. Due to the short time period of simulations, models also fail to calculate a reliable CO_2 seasonal cycle as well as stratospheric-tropospheric exchanges. (Shia et al., 2006) concluded that at least three years are required for the surface CO_2 to be transported into the upper troposphere and LMS then moved to the temperate and polar latitudes. In order to eliminate the spurious diffusivity effect, Lagrangian or quasi-Lagrangian models, such as TRACZILLA (Legras et al., 2005) and CLaMS (the Chemical Lagrangian Model of the Stratosphere) (Pommrich et al., 2014), have been widely used to investigate the transport properties. The combination of these Lagrangian models with in situ observations to reconstruct chemical trace gas distributions has significantly contributed to our understanding of the mixing effects across the extra-tropical tropopause (Hoor et al., 2004; Pan et al., 2006; James and Legras, 2009), the filamentary structure in long-lived and short-lived species near the edge of the polar vortex (Konopka et al., 2003), the transport of

long-lived species and CO from the tropical troposphere to the stratosphere (Pommrich et al., 2014) and on the processes that control UTLS composition (Riese et al., 2012).

The small-scale variability of CO_2, its strong gradients across the tropopause and the scarcity of suitable observations for validation purposes lead to a challenging task for CTMs and CCMs to reconstruct its distribution in the UTLS (Hegglin et al., 2008).

In this paper our goal is to build a database of the monthly mean, zonal mean distribution of CO_2 at global scale extending from the upper troposphere to stratosphere using backward Lagrangian trajectories. This product can be used to validate CTMs, CCMs, as a prior for inversion modelling and to analyse features of the stratospheric-tropospheric exchange as well as the stratospheric circulation and its variability.

The trajectory data set on which this work is based has been used by Diallo et al. (2012) to study the age of air and its variability in the stratosphere. We refer to this previous work for all related questions. The present study can also be seen as a further validation of Diallo et al. (2012).

We reconstruct a global distribution of CO_2 calculated over the time period 2000–2010 from a Lagrangian transport model driven by horizontal winds and diabatic heating rates, which are the vertical velocity in isentropic coordinate, from the ERA-Interim reanalysis povided by the European Centre for Medium Range Weather Forecast (ECMWF) (Dee et al., 2011). We describe the data and method used in this study in Sect. 2 and Sect. 3, respectively. The reconstructed CO_2 is compared with observations in Sect. 4. The global monthly distribution of the zonal mean CO_2 and its variability are discussed in Sect. 5. Finally, section section 6 provides further discussions and conclusions.

2 Data

The reconstruction of the global distribution of CO_2 from the upper troposphere to the stratosphere through the use of back trajectories requires the value of the CO_2 mixing ratio to be assigned at the lower tropospheric boundary. This is achieved by using two different types of CO_2 data: ground stations (Worden et al., 2015) and CarbonTracker (Peters et al., 2007). In

addition, in situ measurements of CO_2 from balloon and aircraft have been used to validate the reliability of the model reconstructions.

2.1 Lower boundary condition of the backward trajectories

Two different observation-based data sets are used to assign CO_2 to the backward trajectories in the Lagrangian model depending on the time period considered. During the 1989–1999 time period, data from ground stations of the World Data Centre for Greenhouse Gases (WDCGG, http://ds.data.jma.go.jp/gmd/wdcgg/) are used to assign a CO_2 mixing ratio to the backward integrated air parcels. The WDCGG is an international data center participating in WMO Global Atmosphere Watch. It provides extensive data from ground stations and aircraft measurements across the Earth that are non-homogeneously distributed. The monthly CO_2 data from ground stations (e.g. Mauna Loa, South Pole and others) located at different latitudes have been used to overcome the daily fluctuations of CO_2 in the atmospheric boundary layer. The criterion to select the ground stations is that the elevation is high enough to neglect the variability due to localized sources at ground level. The CO_2 data are averaged from pole to pole in latitude increments of 30° and over all longitudes to represent the global, free tropospheric CO_2 field. To better model the latitude dependence of the seasonal cycle and to overcome discontinuities, the averaged CO_2 data obtained are then interpolated linearly along the latitude. Since the ground station locations are inadequate to define longitudinal variability we use a constant CO_2 value at all longitudes for each latitude bin. This is our baseline for injecting CO_2 mixing ratio to constrain the backward trajectories from the model during the 1989–1999 time period.

During the 2000–2010 time period we use CO_2 output from the coupled data assimilation system CarbonTracker with the TM5 transport model for the lower boundary condition (Huijnen et al., 2010). CarbonTracker produces full three dimensional output so the back trajectories are assigned daily CO_2 mole fractions based on the latitude and longitude ($3^\circ \times 2^\circ$resolution) of the trajectory at the $5\,\mathrm{km}$ ($500\,\mathrm{hPa}$) level. The $5\,\mathrm{km}$ level was chosen to represent the well mixed free troposphere. CarbonTracker system assimilates CO_2 observations from atmospheric stations and optimizes underlying fluxes ocean, biosphere, biomass burning and fossil fuel usage. These data are meant to achieve a complete and realistic diagnostic of the lower atmo-

spheric CO_2 and fluxes (CarbonTracker-2013B, www.esrl.noaa.gov/gmd/ccgg/carbontracker/). The version used in this study corrects an error in vertical mixing in the previous versions.

Admittedly, the reduced sampling of the pre-2000 period and the lack of zonal variability induces an increased uncertianty in our calculation. However, the zonal variability is largely filtered out in the upper troposphere and lower stratosphere, especially during winter. Moreover, we only provide $CO-2$ reconstructions for 2000–2010. From the beginning of this period, the tropospheric conditions are mostly determined by CarbonTracker date due to the fast transport time in the troposphere and the zonal fluctuations are mostly washed out in the stratosphere. The influence of pre-2000 data then decays exponentially and almost vanishes after 2005.

2.2 *In situ* aircraft and balloon measurements

In the UTLS, there are strong horizontal and vertical gradients. These gradients may occur on a small scale and exhibit a high temporal and spatial variability. In this study, we are interested in airborne measurements to validate our model as well as to characterize the stratospheric variability and mixing process. Aircraft observations have a vertical resolution of a few meters (during ascents and descents) and a horizontal resolution of a few hundred meters resulting from the high sampling frequency of these instruments (0.5–2 Hz). Therefore, the aircraft observations are able to sample the small-scale variability of the tracers.

The SAGE III Ozone Loss and Validation Experiment (SOLVE) sought to establish a comprehensive data set of UTLS trace gases and meteorological data in the Northern polar regions, including latitudinal gradients across the polar vortex . Measurements were made in the Arctic high-latitude region during winter 1999–2000 using the NASA DC-8 and ER-2 aircrafts, as well as balloon platforms and ground-based instruments. CO_2, CH_4 and N_2O were measured by several instruments and used to calculate a composite mean age (as in Andrews et al. (2001b), using earlier measurements).

In situ balloon-based CO_2 profile measurements are also used as basis for comparisons with the reconstructed CO_2 from the Lagrangian transport model. The data sets used in this study are high-quality observations with sufficient altitude coverage. They are measurements of whole air samples collected cryogenically from balloons or in situ measurements on-board a balloon

gondola (Engel et al., 2009; Ray et al., 2014). Four balloon flights have been selected for which a full CO_2 profile is available: (1) at Ft. Sumner, New Mexico, USA (34.5°N) on 17 September 2004, (2) at Sanriku, Japan (39.33°N) on 30 May 2001, (3 and 4) at Aire sur L'Adour, France (43.75°N) on 24 September 2002 and on 9 October 2001, respectively. Note that most profile observations are from the May to October period, when stratospheric variability in the northern hemisphere is expected to be lower than during the winter period. The combined measurements of CO_2 and SF_6 has been used by Engel et al. (2009) to derive the mean age of air but here we focus on CO_2.

A further data set, based on the CONTRAIL experiment (Machida et al., 2008) has been used in the validation process of the reconstructed CO_2 in the whole troposphere (6–13 km) from 20°S to 60°N during November 2005–2009, in particular, near the tropospheric boundary condition as well as near the tropical tropopause layer. The CO_2 mixing ratio has been measured during the regular flights of the Japan Airlines from Japan to Australia, Europe, North America, and Asia with a Continuous Measuring Equipment (CME) for in situ CO_2 observations, as well as an improved Automatic air Sampling Equipment (ASE) for flask sampling [for more details about the instrument see Machida et al. (2002)]. This data set provides significant spatial coverage particularly in the northern hemisphere (Sawa et al., 2008).

3 Method of global CO_2 reconstruction

In order to calculate the global CO_2 distribution, air particles are distributed from the upper troposphere to the stratosphere and backward integrated in time.

3.1 Global backward trajectory

Backward deterministic trajectories are calculated using the Lagrangian transport model, TRACZILLA, (Legras et al., 2005), which is a modified version of FLEXPART (Stohl et al., 2005). TRACZILLA uses analysed winds to move particles in the horizontal direction and performs direct interpolation from data on hybrid levels. In the vertical direction, we have used

potential temperature coordinate and total heating rates. We denote the trajectories as diabatic following a convention established by Eluszkiewicz et al. (2000). At each level in the vertical, trajectories are initially distributed over a longitude-latitude grid with 2° resolution in latitude and an almost uniform spacing in longitude of $2°/\cos(\phi)$, where ϕ is the latitude, generating 10 255 particles on each level from pole to pole. In the sake of simplicity, the vertical levels of the initial grid are chosen to be the hybrid levels of the ECMWF model. In order to encompass the whole stratosphere at any latitude, the 30 levels from about 400 hPa (varying according to the surface pressure) to 2 hPa are selected. Above 56 hPa, the hybrid levels reduce to pure pressure levels. Trajectories starting below the tropospheric boundary condition at 500 hPa, at which we assign the free tropospheric $\mathrm{CO_2}$ to each trajectory, are discarded during the initialization. Trajectories starting above this boundary are integrated backward in time up to 10 years or until they cross the boundary. In practice stratospheric trajectories reach this boundary shortly (less than two months) after crossing the tropopause. Ensembles of trajectories were launched at the end of every month over the period 2000–2010 (Diallo et al., 2012).

3.2 Calculation of the global $\mathrm{CO_2}$

Once a parcel has reached the tropospheric boundary condition at 500 hPa at a given time and a given location, its $\mathrm{CO_2}$ mixing ratio is assigned according to the mixing ratio at that time and that location calculated from CarbonTracker and WDCGG. CarbonTracker is chosen when the tropospheric boundary is impacted after 1st January 2000 and WDCGG is chosen when it is impacted before this date. Since WDCGG provides surface data only it is assumed that the vertical transport is fast in the lower troposphere and induces only a negligible bias at 500 hPa in $\mathrm{CO_2}$ mixing ratio, which is well verified (not shown) in the inner tropical region where most parcels reach the boundary. The assigned value is then used to reconstruct the $\mathrm{CO_2}$ mixing ratio at the location and time of the trajectory initialization.

The zonal mean, monthly mean $\mathrm{CO_2}$ for a given bin in latitude and altitude is calculated as the average over all longitudes of the trajectories initialized within this bin (Fig. 1). The latitudinal resolution of the bins is centered 2° equatorward of 68° and decreases near the poles (69°–73°, 73°–77°, 77°–81°, 81°–90°). For each date, the average is made over 180 particles at the

equator and 67 particles at 68° N or S. Near the poles, towards which the number of trajectories launched per degree of latitude decreases to zero, larger intervals are chosen to maintain a large enough number of trajectories in the bins. This calculation uses the same approach as Sect. 2.3 of Diallo et al. (2012). Further averaging over time is performed to improve statistics and to reduce noise. These averaging procedures are a simple way to account for mixing in the stratosphere and gather within each bin a distribution of particles with different histories.

As observed by Scheele et al. (2005), the number of backward trajectories launched at a given date and that remain within the stratosphere after some delay time residence τ, decreases exponentially with τ. Figure 1 in Diallo et al. (2012) shows that this law is indeed very well satisfied for $\tau > 3\mathrm{yr}$ with an exponential decrement $b = 0.2038\mathrm{yr}^{-1}$ using ERA-Interim winds and heating rates and that the standard deviation from the mean (when each month is considered separately) decays at the same rate. After 10 years of backward motion, 88 % of the particles launched within the stratosphere have met the tropopause and entered the troposphere. We follow Scheele et al. (2005) in using this property to correct the estimated CO_2 for the truncation of trajectory lengths at 10 years. If we define $G(J|t,\tau)$ as the probability density of the residence time τ at time t for parcels launched in the bin J, the monthly mean stratospheric CO_2 mixing ratio is

$$\overline{\mathrm{CO_2}(J,t)} = \int_0^\infty {\mathrm{CO_2}}^T(t-\tau)G(J|t,\tau)d\tau. \quad (1)$$

where ${\mathrm{CO_2}}^T$ is the tropospheric mixing ratio of CO_2 which is assumed here uniform for simplicity. The truncated version of this integral, up to $t_f = 10\mathrm{yr}$, can be calculated explicitly from the backward trajectories as a mean for all parcels from bin J which have hit the 500 hPa surface weighted by their proportion among all launched parcels in bin J. Assuming that $G(J|t,\tau) = G(J|t,t_f)\exp\big(-b(\tau-t_f)\big)$ for $t > t_f$ with ${\mathrm{CO_2}}^T$ governed by an annual modulation added to a linear growth, ${\mathrm{CO_2}}^T(\tau) = p_0 + p_1\cdot\tau + a_0\cdot\cos\big(2\pi(\tau-\varphi)\big)$, the monthly mean CO_2 mixing ratio can be estimated as

$$\overline{\mathrm{CO_2}}(J,t) = \int_0^{t_f} {\mathrm{CO_2}}^T(t-\tau) G(J|t,\tau) d\tau + \frac{G(J|t,t_f)}{b} \left\{ \left(p_0 + p_1(t-t_f-\frac{1}{b}) \right) + \frac{b a_0}{b^2+4\pi^2} \left[b\cos(2\pi(t-t_f-\varphi)) + 2\pi\sin(2\pi(t-t_f-\varphi)) \right] \right\}. \quad (2)$$

where all times are in year. The contribution of remaining particles after 10 years of backward motion is thus accounted by the integrated term in Eq. (2) where $G(J|t,t_f)/b$ is the proportion of parcels in the bin which have not hit the 500 hPa surface at time t_f. The coefficients $\{p0,p1,a_0,\varphi\}$ are estimated by fitting the Mauna Loa $\mathrm{CO_2}$ data. The correction can be applied also below the tropopause as the only tropospheric parcels which live 10 yr without hitting the 500 hPa surface are among those which have been entrained in the stratosphere.

3.3 Evaluations of the global reconstruction method

The reconstruction during SOLVE and in situ balloon campaigns are used for evaluation of the global reconstruction of $\mathrm{CO_2}$ and the ability of TRACZILLA to reproduce the small scale $\mathrm{CO_2}$ variations along the flight tracks.

3.3.1 Reconstruction of $\mathrm{CO_2}$ along aircraft flight track and balloon profiles

The procedure used here differs from that of the global reconstruction described above in three main respects. First the parcels are initialized at locations distributed along the flight track or the balloon profile. In the case of the ER-2 flights, parcels are released with the frequency of the measurement, that is at 0.25 Hz (Daube et al., 2002), that is 900 locations per flight hour. In the case of the balloon flight (Engel et al., 2009), the particles are distributed along the balloon profile with a frequency higher than the tracer measurements. Namely they are released at 200 locations in the vertical regularly distributed in log-pressure between 500 hPa and 1 hPa at the same latitude-longitude position as the balloon.

Second, we take into account that a single trajectory processed by the measurement instruments is in fact a mixture of sub-parcels coming from a large number of origins. The simplest

representation of this mixing is by a constant diffusion, which is mainly acting in the vertical direction, and it is well known that such a process can be represented by a Wiener process. Therefore, following Legras et al. (2005), we release from each release location a large number of parcels (200 for the ER-2 flights, 5000 for the balloon profiles) and the Lagrangian advection is modified such that on a time step δt the motion of a given parcel located in $\mathbf{X}$ is

$$\delta \mathbf{X} = \mathbf{u}(\mathbf{X},t)\delta t + \delta\eta \mathbf{k} \tag{3}$$

where $\mathbf{k}$ is the vertical unit vector and $\delta\eta \equiv w(t)\delta t$ is the product of the time step δt and a Wiener process w approximated by 50 iterations of a white noise during a time step. In the small δt limit, this is equivalent to a diffusion $D = \frac{1}{2} < w^2 > \delta t$. The well-posedness in the backward time direction arises from the adjoint equation of the Green function of advection-diffusion [more details see Legras et al. (2005)]. The value D in the lower stratosphere has been estimated (Legras et al., 2005; Pisso and Legras, 2008) by comparing the observed tracer small-scale fluctuations and their reconstructions. The resulting value is $D \approx 0.1 \mathrm{m^2 s^{-1}}$ which is applied to the whole atmosphere in the present study. Physically, this turbulent diffusion which is about four orders of magnitude larger than the molecular diffusion of $\mathrm{CO_2}$ in the air (Haynes and Lide, 2012, 1.6 $10^{-5}\,\mathrm{m^2 s^{-1}}$) accounts for the small-scale motion missing in the ERA-Interim reanalysis winds. It is noticeable that the diffusion is effective at dispersing the clouds of parcels emitted from a single location only for a few days, after which dispersion by the resolved wind strain dominates.

Third, the trajectories are integrating backward for six months after which the $\mathrm{CO_2}$ mixing ratio is assigned according to the zonal mean value calculated from the global reconstruction at that time and at the locations of the parcels. The mean value is then calculated at each location over all the launched particles and the confidence interval can be estimated as well. The parcels which have reached the $500\,\mathrm{hPa}$ boundary in the mean time are assigned as they hit this surface.

4 Comparison of observations and model reconstructions

In this section, we test the realism of CO_2 reconstructions against several observation data sets that span a large range of scales, geographical locations and altitudes.

4.1 SOLVE campaign

Fig. 2 compares the observed (Daube et al., 2002) and the reconstructed CO_2 mixing ratio for all the exploitable flights of the SOLVE campaign. Fig. 3 shows the same comparison in a tracer-tracer diagram with display of the correlations and of the mean distance Δ between the observed and the reconstructed curves defined for each flight as the sum of the absolute difference between the observed and the reconstructed values divided by the number of recorded values. Fig. 3 shows the same comparison in a tracer-tracer diagram with display of the correlations. The flights patterns include tests flights at subtropical (11^{th} December 1999, 16^{th} December 1999, 06^{th} January 2000) and mid latitudes (11^{th} January 2000), transit flights between mid and high latitudes (14^{th} January 2000, 16^{th} March 2000), flights inside the polar vortex or across its edge (all other dates). In all cases but except very few, the observed CO_2 falls within the 95% confidence interval of the reconstruction. It can be seen from Fig. 3 that the correlation is not a good indicator of the similarity between the observed and the reconstructed curves as it can be high due to trends even for cases that exhibit large differences like 3^{th} February 2000. The Δ value is a much better metric of the distance. In 6 cases out of 16, the agreement is excellent with $\Delta \leq 0.36$ and the two curves almost superimpose but for small-scale fluctuations. In four other cases with $0.49 \leq \Delta \leq 0.61$ the two curves stay very close but for a couple of features are missed by the reconstruction. In two other cases with $0.66 \leq \Delta \leq 0.67$ the reconstruction shows some larger deviation from the observation. On 11^{th} December 1999, the reconstruction misses the decrease of CO_2 as the plane rises at the beginning of the flight and then stays slightly above for the following horizontal lag. The 27^{th} January 2000 case is a flight from the inside of the polar vortex to the outside which is badly reconstructed for the outside part between 10:30UTC and 13UTC. Using similar methods, Legras et al. (2005) showed that stratospheric tracers O_3 and N_2O could be reconstructed for this flight but also found a large

standard deviation for the outside section where filaments or polar and extra-tropical air where interleaved. On four cases with $\Delta > 0.74$, the discrepancy is larger. The discrepancies on 14^{th} January 2000, 03^{th} February 2000, 07^{th} March 2000 and 16^{th} March 2000 can be explained by flight tracks following the edge of the vortex. In such cases, the reconstructions is highly sensitive to the misplacement of the vortex edge in the reanalysis and these cases can hardly be used as a reference.

In addition, it is important to notice that the unique applied diffusion $D \approx 0.1\,\mathrm{m^2 s^{-1}}$ is able to fit well the amount of small-scale spatial variability (at scales down to $1\,\mathrm{km}$) which is displayed by the observations. See Legras et al. (2005) for a complete discussion on this matter.

4.2 Balloon vertical profiles

In order to test the reconstruction over a larger vertical range in altitude, Fig. 4 shows the comparison of the vertical profiles of the reconstructed mean CO_2 by TRACZILLA with the observations of four mid latitude stratospheric balloon flights (Engel et al., 2009; Ray et al., 2014). For three of the cases, most of the measurements fall within the 95% confidence interval of the reconstructed profiles and the local maxima at 23 and $18\,\mathrm{km}$ on the panels c and d, respectively, are well reproduced. These three profiles have in common a high CO_2 values in the troposphere, which decrease with altitude. However, the reconstructed profile on the panel b is shifted on the average to lower values by $1\,\mathrm{ppmv}$ with respect to the observed profile and misses the large fluctuations in this profile above $20\,\mathrm{km}$. This flight was performed from Aire sur l'Adour (France) while a cold front was crossing the area with strong local tracer gradients in the lower stratosphere as seen in the potential vorticity map shown in the panel. This is a likely explanation of the large spread of the observations and the shift in the reconstruction as already seen, for a similar case by Pisso and Legras (2008) (see their figures 9 and 10).

Fig.4 also illustrates the increase of the stratospheric CO_2 from 2001 (a) to 2005 (d).

4.3 Temporal series

To obtain additional details about the upward propagation of the tropospheric CO_2 seasonal cycle into the LMS and to evaluate the model near the lower boundary condition and the tropical tropopause, we compare the timeseries of the reconstructed monthly mean CO_2 (Sect. 3.2) with the observations.

Fig. 5a compares the time series of modelled monthly mean CO_2 with the measurements from CONTRAIL (Sawa et al., 2008, 2012) in the tropical region 10°S–20°N and in the vertical range 7–9 km between November 2006 and January 2010. The comparison shows the ability of the model to capture the tropospheric CO_2 seasonal variation and validates the tropospheric boundary condition.

Fig. 5b compares the modelled monthly mean CO_2 time series in a year at the altitude bin 16–17 km and between 10°S and 20°N just below the tropical tropopause, where the tropospheric air enters the stratosphere, with the average of ground-based CO_2 data from Mauna Loa (19 °N) and American Samoa (14 °S) delayed by 15 days. We find, consistently with Boering et al. (1996) and Andrews et al. (1999, 2001a,b), that the amplitude of the two signals is the same and we recover a delay of 2 months at higher altitude in the layer 18–19 km (not shown) in agreement with Boering et al. (1996). The shorter time scale below the tropopause is in agreement with other studies (Bergman et al., 2012; Tissier and Legras, 2016).

Fig. 5c shows the modelled monthly mean CO_2 in the latitude bin 50–60°N at different altitudes in the range 7–13 km between November 2005 and January 2010. These curves are compared with CONTRAIL measurements in the same latitude band (Sawa et al., 2008). The modelled and measured CO_2 differ by less than 1 ppmv except for a few isolated months like March 2006 and March 2009 and outliers like April at 12–13 km. There is a shift of the order of 4–6 months of the mean CO_2 seasonal cycle above 11–12 km, in the lowermost extra-tropical stratosphere, with respect to the tropospheric signal. This is due to the delay induced by the shallow branch of the BDC also found by Bönisch et al. (2009) and Sawa et al. (2008). The discrepancies are concentrated during the spring season during which large gradients of CO_2 span the region, as discussed in Sect. 5.

5 Global distribution of the zonal mean CO_2

The zonal mean distribution of CO_2 illustrates the main features of the BDC, such as mixing and transport variabilities through temporal and spatial evolution. Figure 6 illustrates the typical seasonal variation of the monthly mean CO_2 derived from the Lagrangian reconstruction for 2010 as an example among the 11 years.

5.1 Upper-troposphere and Lowermost stratosphere

The zonal mean distribution of CO_2 in the free atmosphere, especially above 5 km, is driven by the large-scale transport processes. Fast quasi-isentropic mixing is combined with upwelling in the tropics and downwelling in the extra-tropical lowermost stratosphere. Fig. 6a shows odd months modelled meridional distribution for 2010. In the northern hemisphere, the tropospheric monthly mean CO_2 is dominated by a strong seasonal cycle reflecting the biospheric activity. The terrestrial vegetation removes the CO_2 by photosynthesis in its growing phase while returns CO_2 to the atmosphere when it dies and decomposes. CO_2 concentration increases during fall and winter to reach a maximum in April-May followed by a rapid decay due to the spring biospheric bloom and reaches a minimum in July-August. The cycle is much weaker in the southern hemisphere and influenced by the transport from the northern hemisphere. The combined effect of fast isentropic mixing (Haynes and Shuckburgh, 2000a,b) and convection (Sawa et al., 2008) propagates the cycle towards the tropics creating both horizontal and vertical gradient (Nakamura et al., 1991; Bönisch et al., 2009; Sawa et al., 2012). It is visible in Fig. 6a that during the northern hemisphere winter the concentration tends to follow the isentropes in the extra-tropics for the potential temperatures up to about 330 K. The barrier effect of the subtropical jet (Miyazaki et al., 2009) generates a strong meridional gradient near 30°N, which is maximum near 350 K. Once it has reached the tropics, CO_2 is then transported upward by tropical convection and propagates into the stratosphere through the BDC. Throughout the summer (June, July and August), while the tropospheric CO_2 is removed from the atmosphere due to the biosphere activity, a layer of high CO_2 extends from the tropics to the northern mid-latitudes into the lower stratosphere driven by the lower branch of the BDC (Bönisch et al., 2008). This

transport is favored by the Asian monsoon anticyclone, which traps young continental air lofted from the surface and induces a flux to the extra-tropical stratosphere on its west side as it is eroded across the jet (Dethof et al., 2000; Bannister et al., 2004; Park et al., 2007b, 2008, 2009, 2010; Randel et al., 2010; Pan et al., 2016). Due to the turnover time of this transport, the maximum concentration of CO_2 in the northern lower stratosphere lags by 4 to 6 months that at the surface and is reached basically when the surface concentration is at its minimum. The result is an inverted vertical profile, which is maximum in July and persists over the summer. A qualitative comparison between the reconstructed CO_2 in Fig. 6a and observations from Sawa et al. (2008) (see their figure 7) exhibits a good agreement in the cycle of the tropospheric and lower stratospheric CO_2 and in particular in the cycle of the inversion. There are, however, differences in the location and intensity of the meridional gradient, which might be due to the specific sampling of Sawa et al. (2008) that generates a strong weight to the most intense region of the Pacific jet stream.

5.2 Middle and upper Stratosphere

Figure 6b shows the CO_2 global distribution in the middle and upper stratosphere up to $42\,\mathrm{km}$ for even months in 2010. As the tropospheric seasonal cycle is transported into the middle and upper stratosphere through the tropical pipe, its amplitude decreases upward because of the combined effect of the upwelling branch of the BDC and mixing processes. The deep branch of the BDC is much slower than the shallow branch and old air with low CO_2 concentrates in the middle and upper stratosphere. Younger air with high CO_2 is isolated in the tropical area, an effect which is maximum during northern hemisphere winter in agreement with age of air calculations (Li et al., 2012; Diallo et al., 2012). The horizontal mixing homogenizes CO_2 in the mid and high latitudes during summer. Because of this prior mixing, the winter containment within the polar vortex generates only a weak polar minimum (and no localized horizontal gradient as we average over latitude circle and not following the CO_2 or potential vorticity contours).

5.3 Uncertainty on the CO_2 global distribution

The Fig. 6c show the 11-monthly average uncertainty on the global distribution of the zonal mean CO_2 which is calculated from the trajectories. The uncertainty is estimated as the standard deviation of the mean by assuming that the contributing trajectories are independent samples. The calculation is performed for each month and the standard deviation is then averaged over 11 years. The estimated CO_2 uncertainties reveal smaller values for the trajectories started in the troposphere than the trajectories started in the stratosphere which have a longer transit time of several years to reach the lower boundary condition where the CO_2 value is assigned. As expected the uncertainty roughly scales with the transit time of the trajectories from the upper troposphere to stratosphere. The maximum uncertainty reaches $1\,\mathrm{ppmv}$ in the stratospheric polar regions where the age is maximum during winter and the sampling is the lowest.

5.4 Spring-Summer vertical profiles

In this section, monthly averaged CO_2 profiles are investigated to better describe the changes in the CO_2 vertical structure within the upper troposphere and stratosphere.

The spring-summer reconstructed vertical profiles of CO_2 are compared with those from the CONTRAIL aircraft measurements for the year 2007 in the 50–60°N latitude range (Fig. 7a). A good agreement is obtained, including for the inversion of the CO_2 vertical profile during August in the lower stratosphere. The monthly mean CO_2 vertical profiles, calculated by backward trajectories, exhibit a complex vertical structure with gradient layers interspersed with no gradient layers.

The annual structure of the profile is made apparent in the Fig. 7b where we show averaged monthly profiles over the period 2000–2010 after removal of the mean CO_2 trend at each level. Starting from January, the increase of CO_2 in the troposphere penetrates upward in the stratosphere over the limited vertical range of the Extra-tropical Transition Layer (Hegglin et al., 2010; Gettelman et al., 2011), that is over 2 to $3\,\mathrm{km}$ above the tropopause as visible on the March profile. Between March and May, another process occurs, which injects young air rich in CO_2 above $13\,\mathrm{km}$. This can only be due to a tropical intrusion favored by the weakening of

the tropical barrier at the end of the winter. The profile suggest (i) that the intrusion is deep from 13 to about 23 km, (ii) that the well-mixed layer between 13 and 16 km is inherited from the well-mixed tropical tropospheric profile at such altitudes and (iii) that the mixing layer between 16 and 23 km is also inherited from the tropical lower stratosphere vertical gradient. The mixing layer persists with the same slope during the whole summer and the bottom of the intrusion corresponds to the maximum of CO_2 when the inversion is at its maximum. During fall, when the subtropical barrier is re-established, the gradient weakens, the residual well-mixed layer disappears and the profile returns to the fairly uniform slope of January.

6 Conclusions

Our study provides a monthly zonal mean distribution of CO_2 spanning the upper troposphere and the stratosphere over the time period 2000–2010, established from observations and the state-of-the-art reanalysis ERA-Interim. The zonal mean distribution of CO_2 is a unique data set of a critical trace gas, that has a variety of usages to validate the representation of upper tropospheric and stratospheric tracer distributions in chemical transport models and chemical climate models, in particular regarding the summer inversion of the CO_2 profile in the northern hemisphere. The data set contains two-dimensional monthly fields gridded on the model's 77 latitudes and 36 vertical levels varying from 90 °S to 90 °N and from 5 to 42 km respectively. This reconstructed monthly zonal mean CO_2 exhibits a remarkable agreement with CONTRAIL data as well as with SOLVE and in situ balloon measurements.

The comparison with SOLVE shows that a Lagrangian-diffusive model is able to reproduce the mean value and the amount of small-scale fluctuations that are recorded by in situ measurements along flight tracks in the lower stratosphere. This reconstruction suggests that the distribution of long-lived tracers, such as CO_2, can be fully explained by the properties of transport as resolved by meteorological analysis or reanalysis and a simple representation of sub-grid scale effects as a diffusion.

In the northern hemisphere troposphere, the monthly mean CO_2 is dominated by biospheric activity and displays a strong seasonal cycle, which is vertically and horizontally propagated to

the tropopause and above in the extra-tropical lowermost stratosphere on the one hand and to the tropics on the other hand, where it reaches the tropopause and enters the stratospheric Brewer-Dobson circulation. In the regions of high horizontal mixing as the mid-latitudes, CO_2 tends to uniformise over isentropic surfaces and its meridional gradients are localized over transport barrier such as the subtropical jet during winter.

Transport of CO_2 into the northern extra-tropical stratosphere above lowermost stratosphere is due to the export of tropical air. The long circuit of CO_2 from the extra-tropics to the tropics in the troposphere and then back to the extra-tropics in the stratosphere induces a time-lag of 4–6 months such that the tropospheric and stratospheric variability are almost in opposition at mid-altitudes. The result is the production of an inverted vertical CO_2 profile during summer. In the mid and upper stratosphere, we have found that as the tropospheric seasonal cycle is transported into the stratosphere through the tropical pipe, its amplitude is smoothed out because of the combined effect of the upwelling branch of the BDC and quasi-horizontal mixing. A more confined tropical pipe is found in the tropical band during the winter and spring than during summer and autumn.

Acknowledgements. We particularly thank Y. Sawa, H. Matsueda and T. Machida for providing CO_2 measurements from CONTRAIL, the ECWMF for providing reanalysis data, WDCGG and its contributors for providing the ground station CO_2 data from 1989–1999, CarbonTracker team for providing the CO_2 data from 2000–2010. We thank Harald Bonisch for comments and helpful discussions. We acknowledge support from the EU 7^{th} framework Program under grant 603557 (StratoClim). M. Diallo was mainly supported by a postdoctoral grant from the ExCirEs Project (CGL2011-24826) funded by the Government of Spain. Further thanks to the CICLAD cluster at the Institut Pierre Simon Laplace in Paris on which most parts of this work had been carried out. The TRACZILLA model CO_2 data set may be requested from the corresponding author (mdiallo@lmd.ens.fr).

References

Abalos, M., Legras, B., Ploeger, F., and Randel, W. J.: Evaluating the advective Brewer-Dobson circulation in three reanalyses for the period 1979–2012, J. Geophys. Res. Atmos., 120, 7534–7554,

doi:10.1002/2015JD023182, 2015.

Andrews, A. E., Boering, K. A., Daube, B. C., Wofsy, S. C., Hintsa, E. J., Weinstock, E. M., and Bui, T. P.: Mean age of stratospheric air derived from in situ observations of CO_2, CH_4 and N_2O, J. Geophys. Res., 106, 32 295–32 314, doi:10.1029/2001JD000465, 1999.

Andrews, A. E., Boering, K. A., Wofsy, S. C., Daube, B. C., Jones, D. B., Alex, S., Loewenstein, M., Podolske, J. R., and Strahan, S. E.: Empirical age spectra for the lower tropical stratosphere from in situ observations of CO_2: Quantitative evidence for a sub-tropical barrier to horizontal transport, J. Geophys. Res., 106, 32,295–32,314, doi:10.1029/2001JD000465, 2001a.

Andrews, A. E., Boering, K. A., Daube, B. C., Wofsy, S. C., Loewenstein, M., Jost, H., Podolske, J. R., Webster, C. R., Herman, R. L., C., S. D., Flesch, G. J., Moyer, E. J., Elkins, J. W., Dutton, G. S., Hurst, D. F., Moore, F. L., Ray, E. A., Romashkin, P. A., and Strahan, S. E.: Mean age of stratospheric air derived from in situ observations of CO_2:Implications for stratospheric transport, J. Geophys. Res., 104, 26 581–26 596, doi:doi:10.1029/1999JD900150, 2001b.

Andrews, D. G., Holton, J. R., and Leovy, C. B.: Middle Atmosphere Dynamics, vol. 40 of *International Geophysics Series*, Academic Press, San Diego, USA, 1987.

Bannister, R. N., O'Neil, A., Gregory, A. R., and Nissen, K. M.: The role of the south-east Asian monsoon and other seasonal features in creating the 'tape-recorder' signal in the Unified Model, Q. J. R. Meteorol. Soc., 130, 1531–1554, doi:10.1256/qj.03.106, 2004.

Bergman, J. W., Jensen, E. J., Pfister, L., and Yang, Q.: Seasonal Differences of Vertical-Transport Efficiency in the Tropical Tropopause Layer: On the Interplay between Tropical Deep Convection, Large-Scale Vertical Ascent, and Horizontal Circulations, Journal of Geophysical Research, 117, D05 302, doi:10.1029/2011JD016992, 2012.

Bernath, P. F., McElroy, C. T., Abrams, M. C., Boone, C. D., Butler, M., Camy-Peyret, C., Carleer, M., Clerbaux, C., Coheur, P.-F., Colin, R., DeCola, P., DeMaziere, M., Drummond, J. R., Dufour, D., Evans, W. F. J., Fast, H., Fussen, D., Gilbert, K., Jennings, D. E., Llewellyn, E. J., Lowe, R. P., Mahieu, E., McConnell, J. C., McHugh, M., McLeod, S. D., Michaud, R., Midwinter, C., Nassar, R., Nichitiu, F., Nowlan, C., Rinsland, C. P., Rochon, Y. J., Rowlands, N., Semeniuk, K., Simon, P., Skelton, R., Sloan, J. J., Soucy, M.-A., Strong, K., Tremblay, P., Turnbull, D., Walker, K. A., Walkty, I., Wardle, D. A., Wehrle, V., Zander, R., and Zou, J.: Atmospheric Chemistry Experiment (ACE): Mission overview, J. Geophys. Res., 32, L15S01, doi:doi:10.1029/2005GL022386, 2005.

Boering, K. A., Wofsy, S. C., Daube, B. C., Schneider, H. R., Loewenstein, M., Podolske, J. R., and Conway, T. J.: Stratospheric mean ages and transport rates from observations of carbon dioxide and nitrous oxide, Science, 274, 1340–1343, doi:10.1126/science.274.5291.1340, 1996.

Bönisch, H. B., Hoor, P., Gurk, C., Feng, W., Chipperfield, M., Engel, A., and Bregman, B.: Model evaluation of CO_2 and SF_6 in the extratropical UT/LS region, J. Geophys. Res., 113, D06 101, doi: 10.1029/2007JD008829, 2008.

Bönisch, H. B., Engel, A., Curtius, H., Birner, T., and Hoor, P.: Quantifying transport into the lowermost stratosphere using simultaneous in-situ measurements of SF_6 and CO_2, Atmos. Chem. Phys., 9, 5905–5919, doi:10.5194/acp-9-5905-2009, 2009.

Bönisch, H. B., Engel, A., Birner, T., Hoor, P., Tarasick, D. W., and Ray, E. A.: On the structural changes in the Brewer-Dobson circulation after 2000, Atmos. Chem. Phys., 11, 3937–3948, doi:10.5194/acp-11-3937-2011, 2011.

Boucher, O., Friedlingstein, P., Collins, B., and Keith P Shine, K. P.: The indirect global warming potential and global temperature change potential due to methane oxidation, Environ. Res. Lett., 4, 044 007, doi:10.1088/1748-9326/4/4/044007, 2009.

Bowman, M., Rozanov, V. V., and Burrows, J. P.: A near-infrared optimized DOAS method for the fast global retrieval of atmospheric CH4, CO, CO2, H2O, and N2O total column amounts from SCIAMACHY Envisat-1 nadir radiances, J. Geophys. Res., 105, 15,231–15,245, doi:10.1029/2000JD900191, 2000.

Butchart, N., Cionni, I., Eyring, V., Shepherd, T. G., Waugh, D. W., Akiyoshi, H., Austin, J., BrÃ¼hl, C., Chipperfield, M. P., Cordero, E., Dameris, M., Deckert, R., Dhomse, S., Frith, S. M., Garcia, R. R., Gettelman, A., Giorgetta, M. A., Kinnison, D. E., Li, F., Mancini, E., McLandress, C., Pawson, S., Pitari, G., Plummer, D. A., Rozanov, E., Sassi, F., Scinocca, J. F., Shibata, K., Steil, B., and Tian, W.: Chemistry-Climate Model simulations of twenty-first century stratospheric climate and circulation changes, J. Climate, 23, 5349–5374, doi:10.1175/2010JCLI3404.1, 2010.

Chedin, A., Hollingsworth, A., Scott, N. A., Serrar, S., Crevoisier, C., and Armante, R.: Annual and seasonal variations of atmospheric CO_2, N_2O and CO concentrations retrieved from NOAA/TOVS satellite observations, Geophys. Res. Lett., 29, 1269, doi:10.1029/2001GL014082, 2002.

Chedin, A., Saunders, R., Hollingsworth, A., Scott, N., Matricardi, M., Etcheto, J., Clerbaux, C., Armante, R., and Crevoisier, C.: The feasibility of monitoring CO_2 from high-resolution infrared sounders, J. Geophys. Res., 108, 4064, doi:10.1029/2001JD001443, 2003a.

Chedin, A., Serrar, S., Scott, N. A., Crevoisier, C., and Armante, R.: First global measurement of midtropospheric CO_2 from NOAA polar satellites: Tropical zone, J. Geophys. Res., 108, 4581, doi: 10.1029/2003JD003439, 2003b.

Daube, B. C. J., Boering, K. A., Andrews, A. E., and Wofsy, S. C.: A High-Precision Fast-Response Airborne CO_2 Analyzer for In Situ Sampling from the Surface to the Middle Stratosphere, J. At-

mos Oceanic Technol., 19, 1532–1543, doi:10.1175/1520-0426(2002)019⟨1532:AHPFRA⟩2.0.CO;2, 2002.

Dee, D. P., Uppala, S. M., Simmons, A. J., Berrisford, P., Poli, P., Kobayashi, S., Andrae, U., Balmaseda, M. A., Balsamo, G., Bauer, P., Bechtold, P., Beljaars, A. C. M., van de Berg, L., Bidlot, J., Bormann, N., Delsol, C., Dragani, R., Fuentes, M., Geer, A. J., Haimberger, L., Healy, S. B., Hersbach, H., Hólm, E. V., Isaksen, L., Kållberg, P., Köhler, M., Matricardi, M., McNally, A. P., Monge-Sanz, B. M., Morcrette, J.-J., Park, B.-K., Peubey, C., de Rosnay, P., Tavolato, C., Thépaut, J.-N., and Vitart, F.: The ERA-Interim reanalysis: configuration and performance of the data assimilation system, Q. J. R. Meteorol. Soc., 137, 553–597, doi:10.1002/qj.828, 2011.

Dethof, A., O'Neill, A., and Slingo, J.: Quantification of the isentropic mass transport across the dynamical tropopause, J. Geophys. Res., 105, 12 279–12 293, doi:10.1029/2000JD900127, 2000.

Diallo, M., Legras, B., and Chédin, A.: Age of stratospheric air in the ERA-Interim, Atmos. Chem. Phys., 12, 12 133–12 154, doi:10.5194/acp-12-12133-2012, 2012.

Eluszkiewicz, J., Hemler, R. S., Mahlman, J. D., Bruhwiler, L., and Takacs, L. L.: Sensitivity of Age-of-Air Calculations to the Choice of Advection Scheme, J. Atmos. Sci., 57, 3185–3201, doi:10.1175/1520-0469(2000)057⟨3185:SOAOAC⟩2.0.CO;2, 2000.

Engel, A., Bönisch, H., Brunner, D., Fischer, H., Franke, H., Günther, G., Gurk, C., Hegglin, M., Hoor, P., Königstedt, R., Krebsbach, M., Maser, R., Parchatka, U., Peter, T., Schell, D., Schiller, C., Schmidt, U., Spelten, N., Szabo, T., Weers, U., Wernli, H., Wetter, T., and Wirth, V.: Highly resolved observations of trace gases in the lowermost stratosphere and upper troposphere from the Spurt project: an overview, Atmos. Chem. Phys., 6, 283–301, doi:10.5194/acp-6-283-2006, 2006.

Engel, A., Möbius, T., Bönisch, H., Schmidt, U., Heinz, R., Levin, I., Atlas, E., Aoki, S., Nakazawa, T., Sugawara, S., Moore, F., Hurst, D., Elkins, J., Schauffler, S., Andrews, A., and Boering, K.: Age of stratospheric air unchanged within uncertainties over the past 30 years, Nature Geoscience, 2, 28–31, doi:10.1038/ngeo388, 2009.

Forster, P. M., Ramaswamy, V., Artaxo, P., Berntsen, T., Betts, R., Fahey, D. W., Haywood, J., Lean, J., Lowe, D. C., Myhre, G., Nganga, J., Prinn, R., Raga, G., Schulz, M., and Van Dorland, R.: Changes in atmospheric constituents and in radiative forcing Climate Change 2007: The Physical Science Basis. Contribution of Working Group I to the Fourth Assessment Report of the Intergovernmental Panel on Climate Change [S. Solomon, D. Qin, M. Manning, Z. Chen, M. Marquis, K.B. Averyt, M.Tignor and H.L. Miller (eds.)], Cambridge University Press, Cambridge, United Kingdom and New York, NY, USA, pp. 129–234, 2007.

Forster, P. M. D. F. and Shine, K. P.: Radiative forcing and temperature trends from stratospheric ozone

changes, Geophys. Res. Lett., 102, 10 841–10 855, doi:10.1029/96JD03510, 1997.

Foucher, P. Y., Chedin, A., Armante, R., Boone, C., Crevoisier, C., and Bernath, P.: Technical Note: Feasibility of CO_2 profile retrieval from limb viewing solar occultation made by the ACE-FTS instrument, Atmos. Chem. Phys., 9, 2873–2890, doi:10.5194/acp-9-2873-2009, 2009.

Foucher, P. Y., Chedin, A., Armante, R., Boone, C., Crevoisier, C., and Bernath, P.: Carbon dioxide atmospheric vertical profiles retrieved from space observation using ACE-FTS solar occultation instrument, Atmos. Chem. Phys., 11, 2455–2470, doi:10.5194/acp-11-2455-2011, 2011.

Frankenberg, C., Pollock, R., Lee, R. A. M., Rosenberg, R., Blavier, J.-F., Crisp, D., O'Dell, C. W., Osterman, G. B., Roehl, C., Wennberg, P. O., and Wunch, D.: The Orbiting Carbon Observatory (OCO-2): spectrometer performance evaluation using pre-launch direct sun measurements, Atmos. Meas. Tech., 8, 301–313, doi:10.5194/amt-8-301-2015, 2015.

Garny, H., Dameris, M., Randel, W., Bodeker, G. E., and Deckert, R.: Dynamically forced increase of tropical upwelling in the lower stratosphere, J. Atmos. Sci., 68, 1214–1233, doi:10.1175/2011JAS3701.1, 2011.

Gettelman, A., Hoor, P., Pan, L. L., Randel, W. J., Hegglin, M. I., and Birner, T.: The extratropical upper troposphere and lower stratosphere, Rev. Geophys., 49, RG3003, doi:10.1029/2011RG000355, 2011.

Gurk, C., Fischer, H., Hoor, P., Lawrence, M. G., Lelieveld, J., and Wernli, H.: Airborne in-situ measurements of vertical, seasonal and latitudinal distributions of carbon dioxide over Europe, Atmos. Chem. Phys., 8, 6395–6403, 2008.

Hammerling, D. M., Michalak, A. M., O'Dell, C., and Kawa, S. R.: Global CO2 distributions over land from the Greenhouse Gases Observing Satellite (GOSAT), Geophys. Res. Lett., 39, L08 804, doi:10.1029/2012GL051203, 2012.

Haynes, P. H. and Shuckburgh, E.: Effective diffusivity as a diagnostic of atmospheric transport 1. Stratosphere, J. Geophys. Res., 105, 22,777–22,794, doi:10.1029/2000JD900093, 2000a.

Haynes, P. H. and Shuckburgh, E.: Effective diffusivity as a diagnostic of atmospheric transport 2. Troposphere and lower stratosphere, J. Geophys. Res., 105, 22 795–22 810, doi:10.1029/2000JD900092, 2000b.

Haynes, W. M. and Lide, D. R., eds.: CRC Handbook of Chemistry and Physics: A Ready-Reference Book of Chemical and Physical Data, CRC Press, Boca Raton, Fla., 93. ed., 2012 - 2013 edn., oCLC: 796257574, 2012.

Hegglin, M. I., Brunner, D., Peter, T., Staehelin, J., Wirth, V., Hoor, P., and Fischer, H.: Determination of eddy diffusivity in the lowermost stratosphere, Geophys. Res. Lett., 32, L13 812, doi:10.1029/2005GL022495, 2005.

Hegglin, M. I., Boone, C. D., Manney, G. L., Shepherd, T. G., Walker, K. A., Bernath, P. F., Daffer, W. H., Hoor, P., and Schiller, C.: Validation of ACE-FTS satellite data in the upper troposphere/lower stratosphere (UTLS) using non-coincident measurements, Atmospheric Chemistry and Physics, 8, 1483–1499, doi:10.5194/acp-8-1483-2008, http://www.atmos-chem-phys.net/8/1483/2008/, 2008.

Hegglin, M. I., Gettelman, A., Hoor, P., Krichevsky, R., Manney, G. L., Pan, L. L., Son, S.-W., Stiller, G., Tilmes, S., Walker, K. A., Eyring, V., Shepherd, T. G., Waugh, D., Akiyoshi, H., nel, J. A. A., Austin, J., Baumgaertner, A., Bekki, S., Braesicke, P., Brúhl, C., Butchart, N., Chipperfield, M., Dameris, M., Dhomse, S., Frith, S., Garny, H., Hardiman, S. C., Jöckel, P., Kinnison, D. E., Lamarque, J. F., Mancini, E., Michou, M., Morgenstern, O., Nakamura, T., Olivié, D., Pawson, S., Pitari, G., Plummer, D. A., Pyle, J. A., Rozanov, E., Scinocca, J. F., Shibata, K., Smale, D., Teyssédre, H., Tian, W., and Yamashia, Y.: Multimodel assessment of the upper troposphere and lower stratosphere: Extratropics, J. Geophys. Res., 115, D00M09, doi:10.1029/2010JD013884, 2010.

Holton, J. R., Haynes, P. H., McIntyre, M. E., Douglass, A. R., Rood, R. B., and Pfister, L.: Stratosphere-troposphere exchange, Rev. Geophys., 33, 403–440, doi:10.1029/95RG02097, 1995.

Hoor, P., Gurk, C., Brunner, D., Hegglin, M. I., Wernli, H., and Fischer, H.: Seasonality and extent of extratropical TST derived from in-situ CO measurements during SPURT, Atmos. Chem. Phys., 4, 1427–1442, 2004.

Hoor, P., Fischer, H., and Lelieveld, J.: Tropical and extratropical tropospheric air in the lowermost stratosphere over Europe: A CO-based budget, Geophys. Res. Lett., 32, L13 812, doi:10.1029/2005GL022495, 2005.

Hoor, P., Wernli, H., Hegglin, M. I., and Bönisch, H.: Transport timescales and tracer properties in the extratropical UTLS, Atmospheric Chemistry and Physics, 10, 7929–7944, doi:10.5194/acp-10-7929-2010, 2010.

Huijnen, V., Williams, J., van Weele, M., van Noije, T., Krol, M., Dentener, F., Segers, A., Houweling, S., Peters, W., de Laat, J., Boersma, F., Bergamaschi, P., van Velthoven, P., Le Sager, P., Eskes, H., Alkemade, F., Scheele, R., Nédélec, P., and Pätz, H.-W.: The global chemistry transport model TM5: description and evaluation of the tropospheric chemistry version 3.0, Geoscientific Model Development, 3, 445–473, doi:10.5194/gmd-3-445-2010, 2010.

James, R. and Legras, B.: Mixing processes and exchanges in the tropical and the subtropical UT/LS, Atmos. Chem. Phys., 9, 25–38, doi:10.5194/acp-9-25-2009, 2009.

Konopka, P., Grooβ, J.-U., Günther, G., McKenna, D. S., Müller, R., Elkins, J., Fahey, D., and Popp, P.: Weak impact of mixing on chlorine deactivation during SOLVE/THESEO 2000: Lagrangian modeling (CLaMS) versus ER-2 in situ observations, J. Geophys. Res., 108(D5), 8324,

doi:10.1029/2001JD000876, 2003.

Lacis, A. A., Wuebbles, D. J., and Logan, J. A.: Radiative forcing of climate by changes in the vertical distribution of ozone, J. Geophys. Res., 95, 9971–9981, doi:10.1029/JD095iD07p09971, 1990.

Legras, B., Pisso, I., Berthet, G., and Lefèvre, F.: Variability of the Lagrangian turbulent diffusion in the lower stratosphere, Atmos. Chem. Phys., 5, 1605–1622, doi:10.5194/acp-5-1605-2005, 2005.

Li, F., Waugh, D. W., Douglass, A. R., Newman, P. A., Pawson, S., Stolarski, R. S., Strahan, S. E., and Nielsen, J. E.: Seasonal variations of stratospheric age spectra in the Goddard Earth Observing System Chemistry Climate Model (GEOSCCM), J. Geophys. Res., 117, 134, doi:10.1029/2011JD016877, 2012.

Li, S. and Waugh, D. W.: Sensitivity of mean age and long-lived tracers to transport parameters in a two-dimensional model, J. Geophys. Res., 104, 30 559–30 569, doi:10.1029/1999JD900913, 1999.

Liu, J., Bowman, K. W., and Henze, D. K.: Source-receptor relationships of column-average CO2 and implications for the impact of observations on flux inversions, J. Geophys. Res., 120, 5214–5236, doi:10.1002/2014JD22914, 2014.

Machida, T., Kita, K., Kondo, Y., Blake, D., Kawakami, S., Inoue, G., and Ogawa, T.: Vertical and Meridional Distributions of the Atmospheric CO $_2$ Mixing Ratio between Northern Midlatitudes and Southern Subtropics, Journal of Geophysical Research, 108, doi:10.1029/2001JD000910, 2002.

Machida, T., Matsueda, H., Sawa, Y., Nakagawa, Y., Hirotani, K., Kondo, N., Goto, K., Nakazawa, T., Ishikawa, K., and Ogawa, T.: Worldwide Measurements of Atmospheric CO $_2$ and Other Trace Gas Species Using Commercial Airlines, Journal of Atmospheric and Oceanic Technology, 25, 1744–1754, doi:10.1175/2008JTECHA1082.1, 2008.

Miyazaki, K., Machida, T., Patra, P. K., Sawa, Y., Matsueda, H., and Nakazawa, T.: Formation mechanisms of latitudinal CO2 gradients in the upper troposphere over the subtropics and tropics, J. Geophys. Res., 114, 2009.

Nakamura, N., Miyashita, K., Aoki, S., and Tanaka, M.: Temporal and spatial variation of upper tropospheric and lower stratospheric carbon dioxide, Tellus, 43B, 106–117, 1991.

Olsen, S. C. and Randerson, J. T.: Differences between surface and column atmospheric CO2 and implications for carbon cycle research, J. Geophys. Res., 109, D02 301, doi:10.1029/2003JD003968, 2004.

Pan, L., Honomichl, S. B., Kinnison, D. E., Abalos, M., Randel, W. J., Bergman, J. W., and Bian, J.: Transport of Chemical Tracers from the Boundary Layer to Stratosphere Associated with the Dynamics of the Asian Summer Monsoon, J. Geophys. Res., pp. 2169–8996, doi:10.1002/2016JD025616, http://dx.doi.org/10.1002/2016JD025616, 2016.

Pan, L. L., Konopka, P., and Browell, E. V.: Observations and model simulations of mixing near the extratropical tropopaus, J. Geophys. Res., 111, D05 106, doi:10.1029/2005JD006480, 2006.

Park, M., Randel, W. J., Gettelman, A., Massie, S. T., and Jiang, J. H.: Transport above the Asian summer monsoon anticyclone inferred from aura microwave limb sounder tracers, J. Geophys. Res., 112, D16 309, doi:10.1029/2006JD008294, 2007b.

Park, M., Randel, W. J., Emmons, L. K., Bernath, P. F., Walker, K. A., and Boone, C. D.: Chemical isolation in the Asian monsoon anticyclone observed in Atmospheric Chemistry Experiment (ACE-FTS) data, Atmos. Chem. Phys., 8, 757–764, doi:10.5194/acp-8-757-2008, 2008.

Park, M., Randel, W. J., Emmons, L. K., and Livesey, N. J.: Transport pathways of carbon monoxide in the Asian summer monsoon diagnosed from Model of Ozone and Related Tracers (MOZART), J. Geophys. Res., 114, D08 303, doi:10.1029/2008JD010621, 2009.

Park, S., Atlas, E. L., Jiménez, R., Daube, B. C., Gottlieb, E. W., Nan, J., Jones, D. B. A., Pfister, L., Conway, T. J., Bui, T. P., Gao, R.-S., and Wofsy, S. C.: Vertical transport rates and concentrations of OH and Cl radicals in the Tropical Tropopause Layer from observations of CO_2 and halocarbons: implications for distributions of long- and short-lived chemical species, Atmos. Chem. Phys., 10, 6669–6684, doi:10.5194/acp-10-6669-2010, 2010.

Peters, W., Jacobson, A. R., Sweeney, C., Andrews, A. E., Conway, T. J., Masarie, K., Miller, J. B., Bruhwiler, L. M. P., Petron, G., Hirsch, A. I., Worthy, D. E. J., van der Werf, G. R., Randerson, J. T., Wennberg, P. O., Krol, M. C., and Tans, P. P.: An atmospheric perspective on North American carbon dioxide exchange: CarbonTracker, Proceed. Nat. Acad. Sc., 104, 18 925–18 930, 2007.

Pisso, I. and Legras, B.: Turbulent vertical diffusivity in the sub-tropical stratosphere, Atmos. Chem. Phys., 8, 697–707, 2008.

Pommrich, R., Müller, R., Grooβ, J.-U., Konopka, P., Ploeger, F., B. Vogel, M. T., Hoppe, C. M., Günther, G., Spelten, N., Hoffmann, L., Pumphrey, H.-C., S. Viciani, F. D., Volk, C. M., Hoor, P., Schlager, H., and Riese, M.: Tropical troposphere to stratosphere transport of carbon monoxide and long-lived trace species in the Chemical Lagrangian Model of the Stratosphere (CLaMS), Geosci. Model Dev., 7, 2895–2916, doi:10.5194/gmd-7-2895-2014, 2014.

Randel, W. J., Park, M., Wu, F., and Livesey, N.: Asian monsoon transport of pollution to the stratosphere, Science, 328(5978), 611–613, doi:10.1126/science.1182274, 2010.

Ray, E. A., Moore, F. L., Rosenlof, K. H., Davis, S. M., Sweeney, C., Bönisch, H., Engel, A., Sugawara, S., Nakazawa, T., and Aoki, S.: Improving stratospheric transport trend analysis based on SF6 and CO2 measurements, J. Geophys. Res., 119, 14 110–14 128, doi:10.1002/2014JD021802, 2014.

Riese, M., Ploeger, F., Rap, A., Vogel, B., Konopka, P., Dameris, M., and Forster, P.: Impact of uncertain-

ties in atmospheric mixing on simulated UTLS composition and related radiative effects, J. Geophys. Res., 117, D16305, doi:10.1029/2012JD017751, 2012.

Salby, M. L. and Callaghan, P. F.: Interaction between the Brewer Dobson Circulation and the Hadley Circulation, Journal of Climate, 18, 4303–4316, doi:10.1175/JCLI3509.1, 2005.

Salby, M. L. and Callaghan, P. F.: Influence of the Brewer-Dobson circulation on stratosphere-troposphere exchange, J. Geophys. Res., 111, D21106, doi:10.1029/2006JD007051, 2006.

Sawa, Y., Machida, T., and Matsueda, H.: Seasonal variations of CO_2 near the tropopause observation by commercial aircraft, J. Geophys. Res., 113, D23 301, 2008.

Sawa, Y., Machida, T., and Matsueda, H.: Aircraft observation of the seasonal variation in the transport of CO_2 in the upper atmosphere, J. Geophys. Res., 117, D05 305, 2012.

Scheele, M., Siegmund, P., and van Velthoven, P.: Stratospheric age of air computed with trajectories based on various 3D-Var and 4D-Var data sets, Atmos. Chem. Phys., 5, 1–7, 2005.

Schuck, T. J., Brenninkmeijer, C. A. M., Slemr, F., Xueref-Remy, I., and Zahn, A.: Greenhouse gas analysis of air samples collected onboard the CARIBIC passenger aircraft, Atmos. Meas. Tech., 2, 449–464, doi:10.5194/amt-2-449-2009, 2009.

Shia, R.-L., Liang, M.-C., Miller, C. E., and Yung, Y. L.: CO2 in the upper troposphere: Influence of stratosphere-troposphere exchange, Geophys. Res. Lett., 33, L14 814, doi:10.1029/2006GL026141, 2006.

Sprung, D. and Zahn, A.: Acetone in the upper troposphere/lowermost stratosphere measured by the CARIBIC passenger aircraft: Distribution, seasonal cycle, and variability, J. Geophys. Res., 115, D16 301, doi:10.1029/2009JD012099, 2010.

Stohl, A., Forster, C., Frank, A., Seibert, P., and Wotawa, G.: Technical note: The Lagrangian particle dispersion model FLEXPART version 6.2, Atmos. Chem. Phys., 5, 2461–2474, doi:10.5194/acp-5-2461-2005, 2005.

Strahan, S., Douglass, A., Nielsen, J. E., and Boering, K. A.: The CO_2 seasonal cycle as a tracer of transport, J. Geophys. Res., D12, 13,729–13,741, doi:10.1029/98JD01143, 1998.

Strahan, S. E., Duncan, B. N., and Hoor, P.: Observationally derived transport diagnostics for the lowermost stratosphere and their application to the GMI chemistry and transport model, Atmospheric Chemistry and Physics, 7, 2435–2445, doi:10.5194/acp-7-2435-2007, 2007.

Tissier, A.-S. and Legras, B.: Convective Sources of Trajectories Traversing the Tropical Tropopause Layer, Atmospheric Chemistry and Physics, 16, 3383–3398, doi:10.5194/acp-16-3383-2016, 2016.

Waugh, D.: Atmospheric dynamics: The age of stratospheric air, Nature Geoscience, 2, 14–16, doi:10.1038/ngeo397, 2009.

Waugh, D. and Hall, T.: Age of stratospheric air: Theory, observations, and models, Rev. Geophys., 40, 1010, doi:10.1029/2000RG000101, 2002.

Worden, J., Noone, D., Galewsky, J., Bailey, A., Bowman, K., Brown, D., Hurley, J., Kulawik, S., Lee, J., and Strong, M.: Analysis based on data submitted by November 2014, except for the greenhouse gas species CO2, CH4, N2O, SF6 and halocarbons, for which the submission period ended in July 2014, WDCGG report, p. 130 pp., 2015.

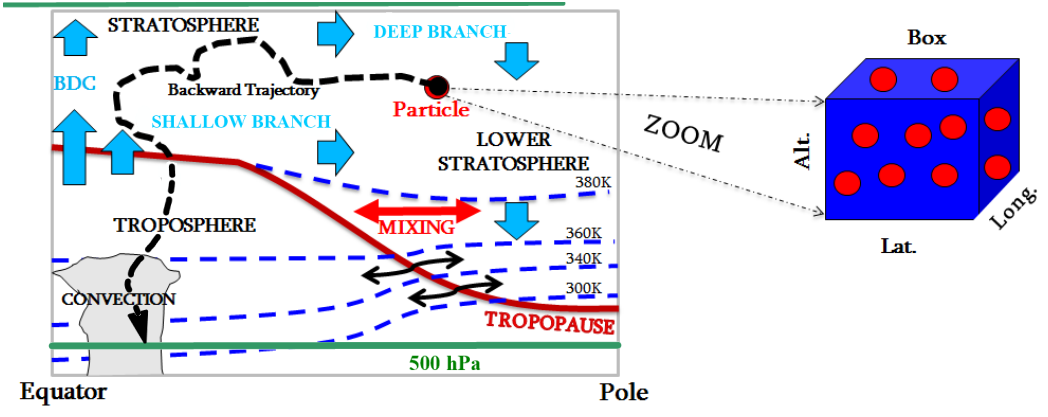

Fig. 1. A schematic representation of the backward Lagrangian trajectories of air particles starting in a (latitude $\times$ longitude $\times$ altitude) grid box. Here the longitudinal extend of the box should be seen as the whole latitudinal circle.

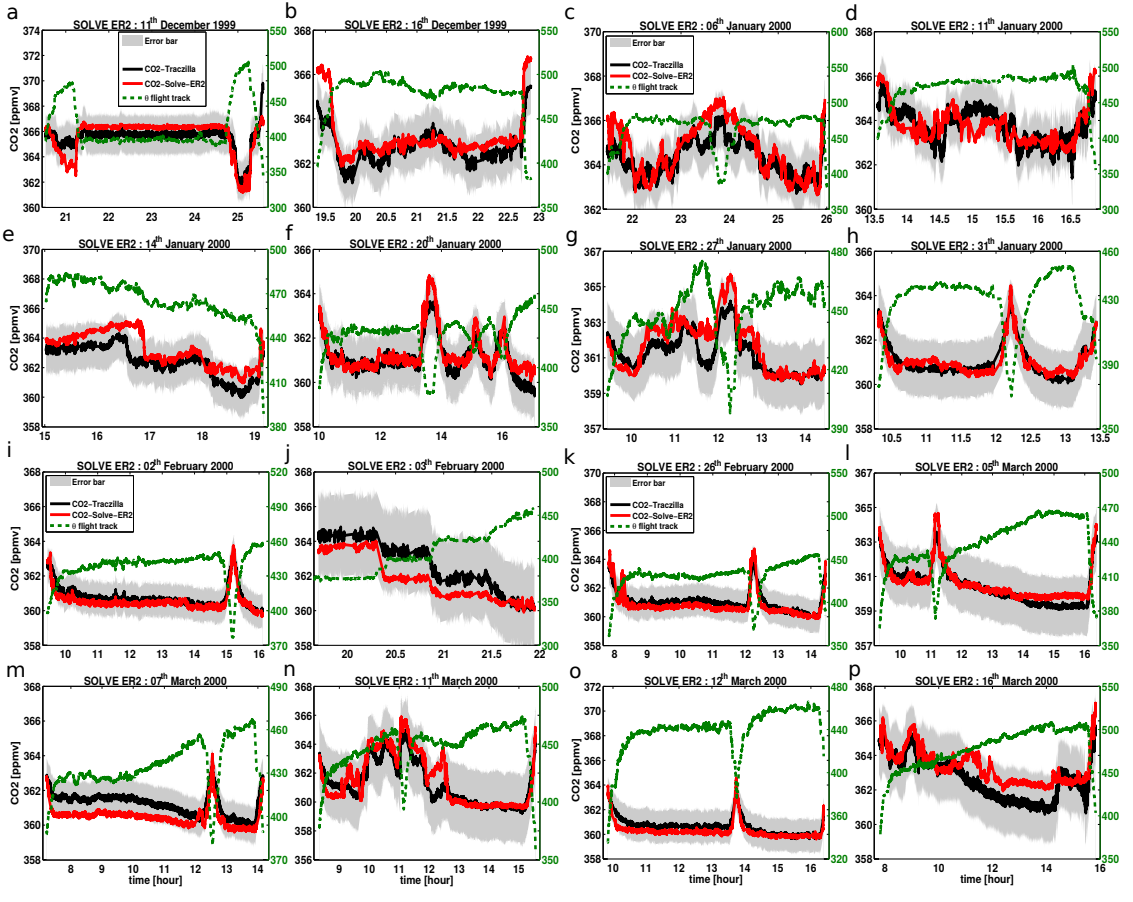

Fig. 2. Comparison of the calculated CO_2 from backward trajectories with aircraft measurements from SOLVE campaign (Daube et al., 2002). (Black): reconstructed CO_2 along the ER-2 flight track using the TRACZILLA Lagrangian transport model. (Red): observed CO_2. (Green): potential temperature of the ER-2 flight track. The gray shading area indicates the 95% confidence interval calculated from the reconstruction.

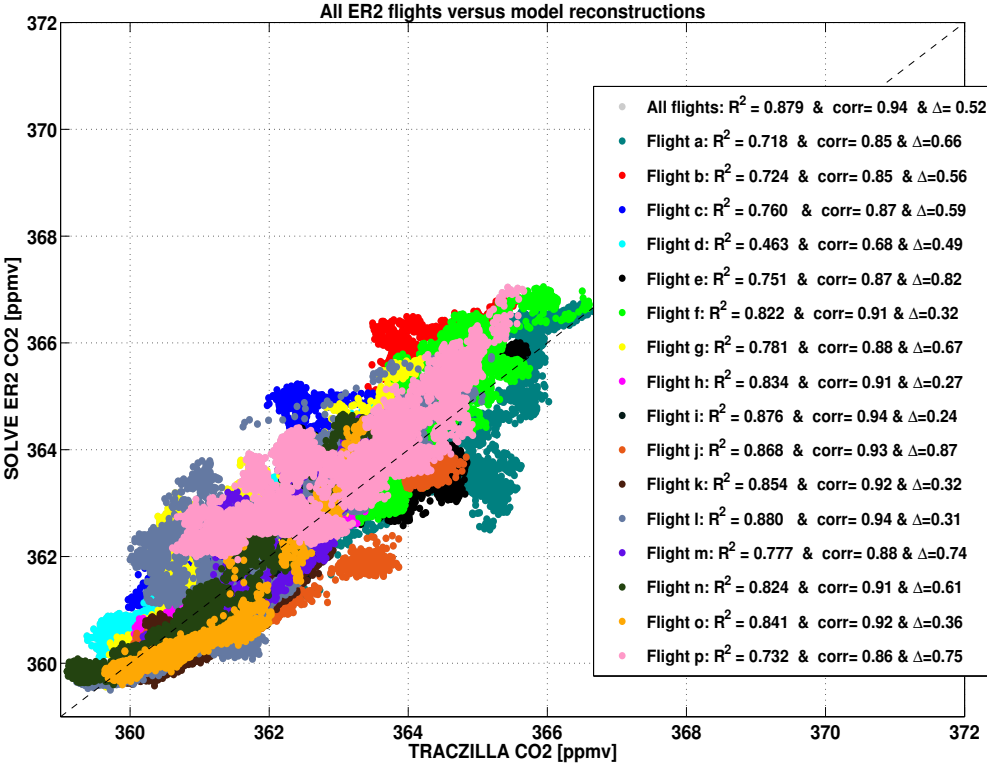

Fig. 3. Comparison of the calculated CO_2 from the backward trajectories with aircraft measurements from SOLVE campaign (Daube et al., 2002). Colors indicate different flights in Fig. 2. R-squared, correlation coefficients and the Δ defined as the mean of the absolute value of model–observations differences are shown in the legend.

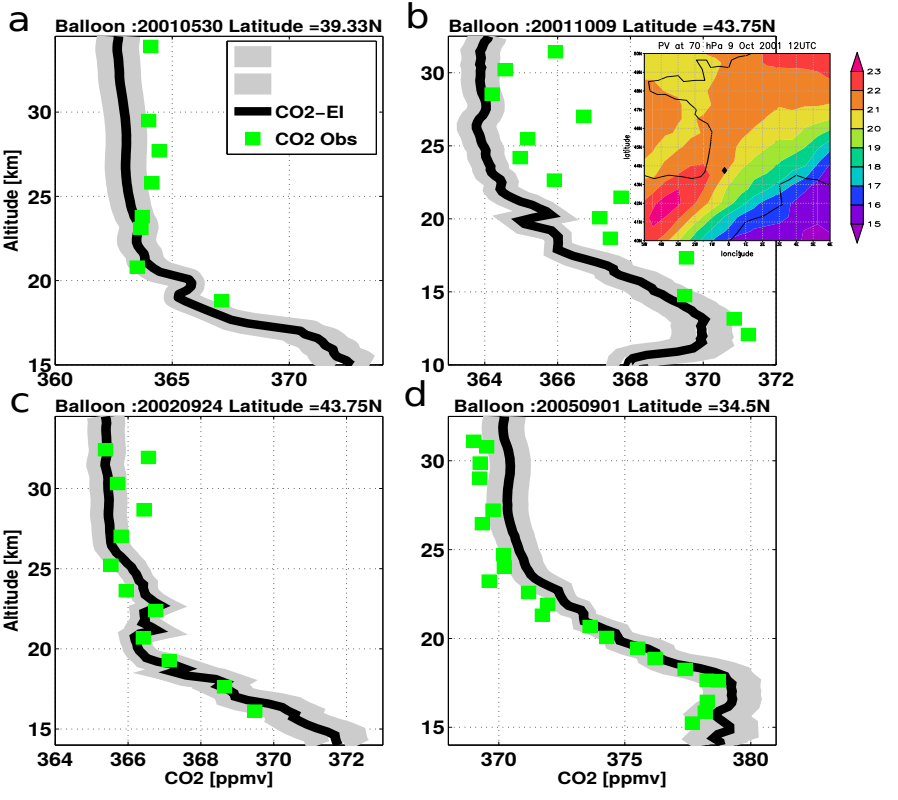

Fig. 4. Reconstructed vertical profiles of the mean CO_2 compared with each *in situ* stratospheric balloon observations of CO_2 (Engel et al., 2009). (Black curves): vertical profiles of mean diabatic CO_2. (Green squares): *in situ* balloon measurements of CO_2. (Gray shading): 95% confidence interval from the reconstruction. The measurements were taken from Sanriku, Japan (39.33 °N) on 30 May 2001 (a), Aire sur l'Adour, France (43.75 °N) on 24 September 2002 (b) and on 9 October 2001 (c) and Ft. Sumner, New Mexico, USA (34.5 °N) on 17 September 2004 (d), respectively. The insert on the upper right panel shows the potential vorticity (in PVU) on the 70 hPa surface for 9 October 2001 at 12UTC over France from ERA-Interim. The location of Aire sur l'Adour is indicated by a diamond.

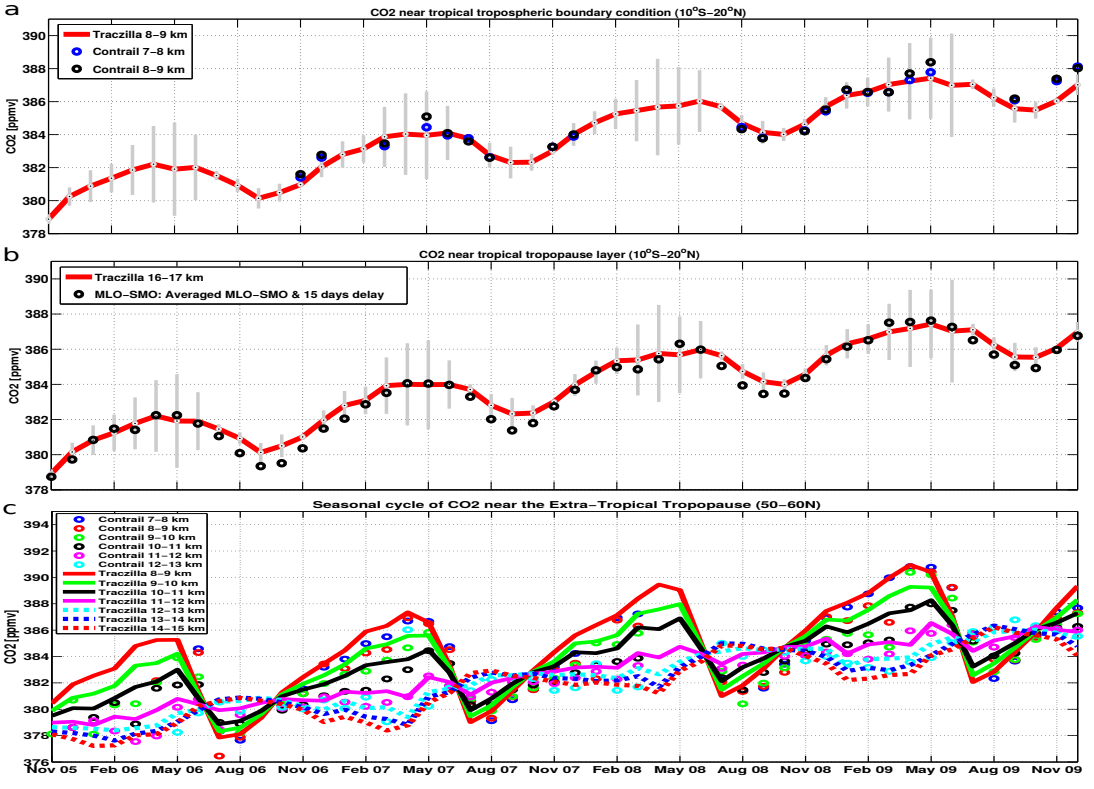

Fig. 5. Temporal evolution of the monthly mean CO_2 seasonal cycle from TRACZILLA calculations (line) compared with CONTRAIL and ground measurements (circle). (a): Comparison model with CONTRAIL in the tropospheric region above the tropospheric boundary in the latitude range 10°S–20°N (b): In the upper tropospheric region close to the tropical tropopause and the latitude range 10°S–20°N, comparison with the average of surface station data at Mauna Loa, Hawaii (19°N) and American Samoa (14°S) delayed by 15 days. (c): Comparison model with CONTRAIL in the upper troposphere near the extra-tropical tropopause at 50°N–60°N and at several heights from 7 to 15 km. The error estimated from the reconstruction is indicated as vertical gray bars.

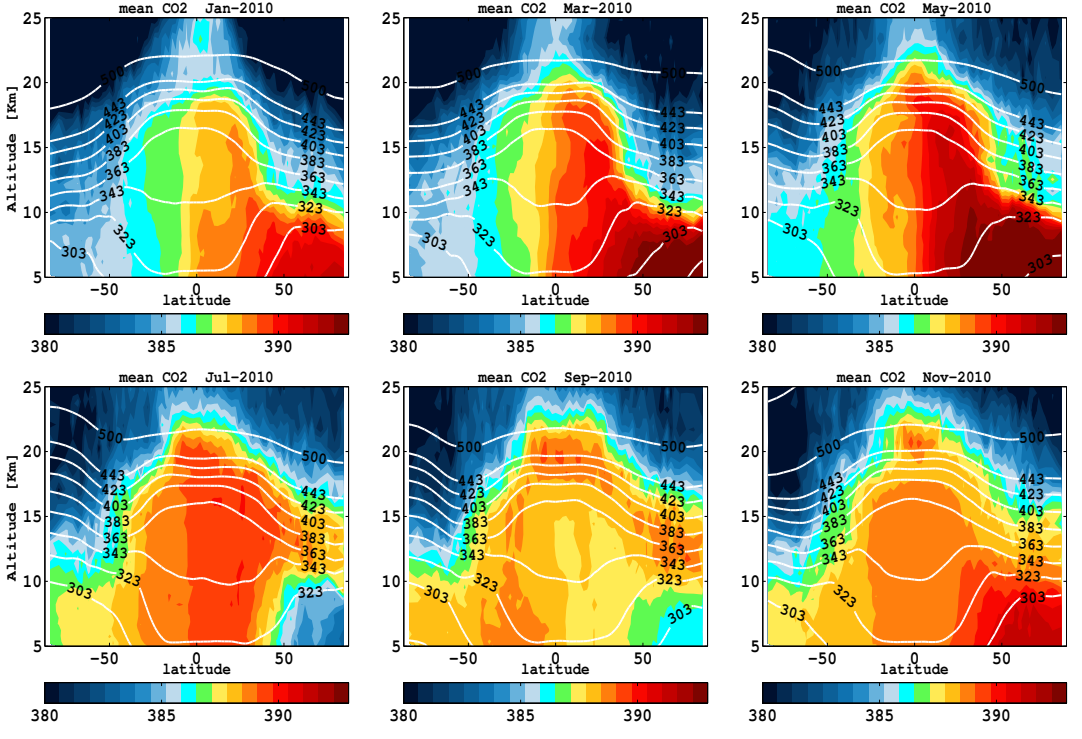
mean CO2 Jan-2010
mean CO2 Mar-2010
mean CO2 May-2010
mean CO2 Jul-2010
mean CO2 Sep-2010
mean CO2 Nov-2010
Altitude [Km]
latitude
25
20
15
10
5
-50
0
50
380
385
390
500
443
423
403
383
363
343
323
303

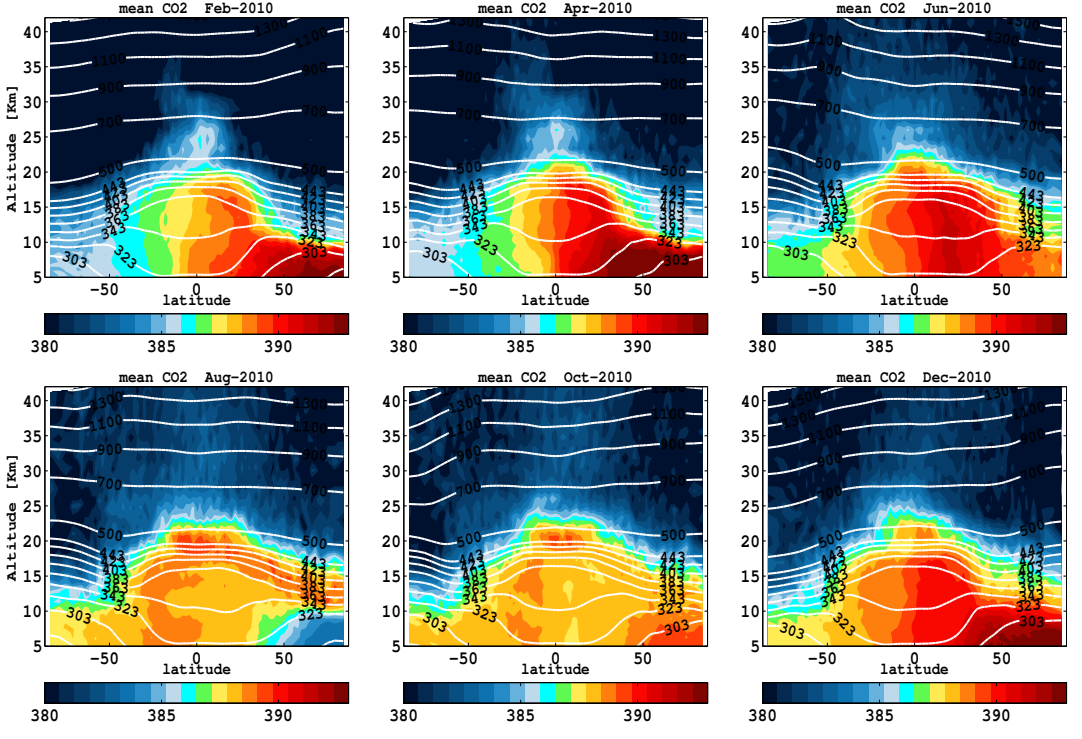
mean CO2 Feb-2010
mean CO2 Apr-2010
mean CO2 Jun-2010
mean CO2 Aug-2010
mean CO2 Oct-2010
mean CO2 Dec-2010
Altitude [Km]
latitude
380
385
390

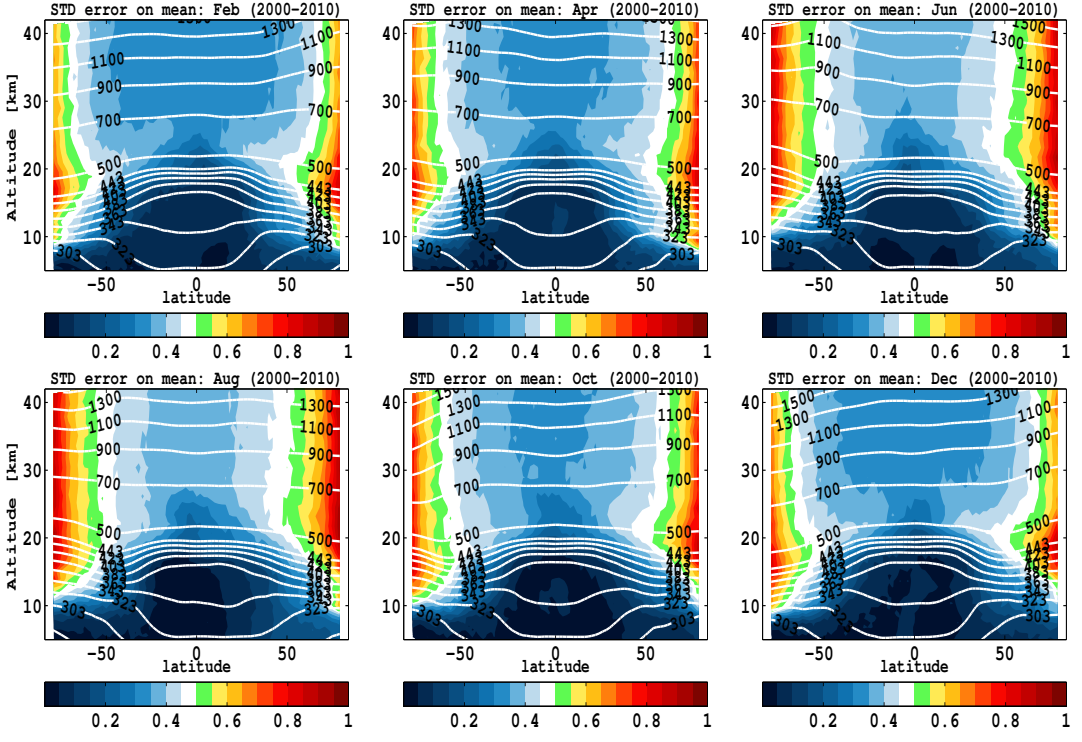

Fig. 6. (a) Global distribution of the seasonal cycle of the mean reconstructed CO_2 (in ppmv) in the upper troposhere and the lower stratosphere from 5 km to 25 km for the odd months of 2010. (b) Same as (a) but for the even months of 2010 and the altitude range from 5 km to 45 km. CO_2 calculated on model levels is first interpolated to altitude levels using the latitude dependency of the zonally and monthly averaged geopotential. (c) The standard deviation error from the mean CO_2 over the 2000–2010 period. The white contours show the isentropic surfaces.

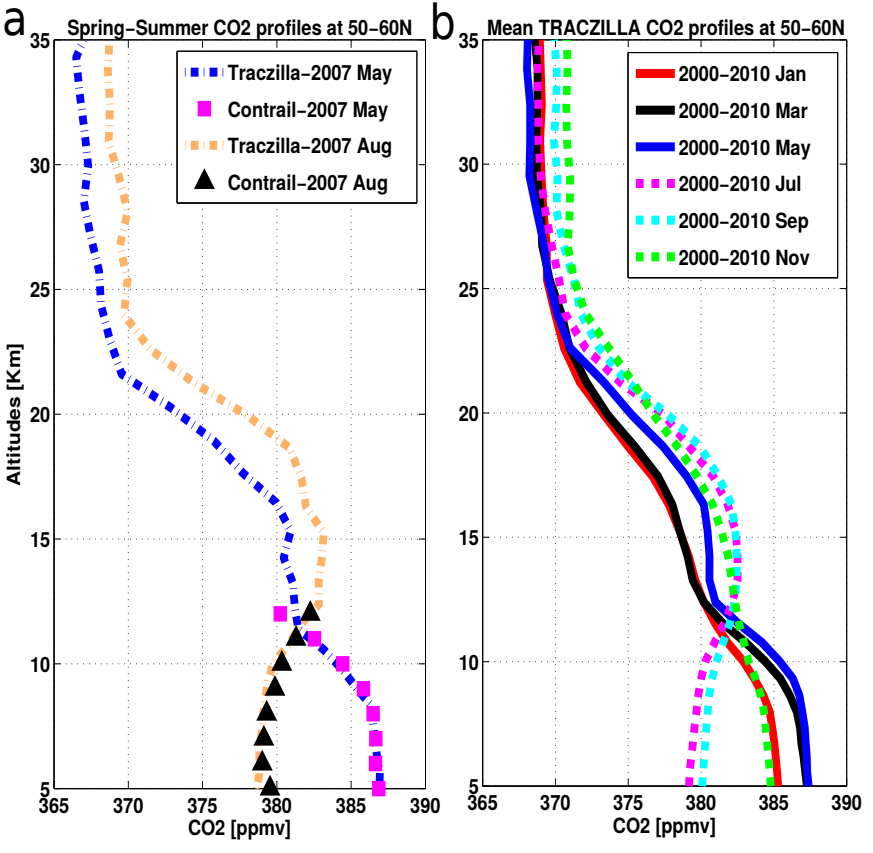

Fig. 7. (a): Reconstructed vertical profiles of the mean CO_2 compared with CONTRAIL measurements for 2007 at 50°N-60°N. (Dotted-dashed lines): vertical profiles of CO_2 from TRACZILLA (blue: May, orange: Aug). (Symbols): *in situ* aircraft measurements from CONTRAIL campaign (magenta square: May, orange triangle: Aug) (b): Averaged monthly profiles of the reconstructed CO_2 over the period 2000–2010 after removal of the mean CO_2 trend at each level and centered on 2007. (red): January, (black): March, (blue): May, (magenta): July, (cyan): September, (green): November.